Bioscience Reports (2022) **42** BSR20211150
https://doi.org/10.1042/BSR20211150

PORTLAND PRESS

Research Article

Effects of DISC1 on Alzheimer's disease cell models assessed by iTRAQ proteomics analysis

Jiajie Lu[1], Rihong Huang[1], Yuecheng Peng[1], Haojian Wang[1], Zejia Feng[1], Yongyang Fan[1], Zhaorong Zeng[1], Yezhong Wang[1], Jiana Wei[2] and Zhaotao Wang[1]

[1]Institute of Neuroscience, Department of Neurosurgery, The Second Affiliated Hospital of Guangzhou Medical University, Guangzhou 510260, China; [2]Institute of Neuroscience, Department of Neurology, The Second Affiliated Hospital of Guangzhou Medical University, Guangzhou 510260, China

Correspondence: Zhaotao Wang (wangzhaotao@gzhmu.edu.cn) or Jiana Wei (923131571@qq.com) or Yezhong Wang (wangyezhong@gzhmu.edu.cn)

Alzheimer's disease (AD) is a form of neurodegenerative disease in the elderly with no cure at present. In a previous study, we found that the scaffold protein, disrupted in Schizophrenia 1 (DISC1) is down-regulated in the AD brains, and ectopic expression of DISC1 can delay the progression of AD by protecting synaptic plasticity and down-regulating BACE1. However, the underlying mechanisms remain not to be elucidated. In the present study, we compared the proteomes of normal and DISC1^{high} AD cells expressing the amyloid precursor protein (APP) using isobaric tag for relative and absolute quantitation (iTRAQ) and mass spectrometry (MS). The differentially expressed proteins (DEPs) were identified, and the protein–protein interaction (PPI) network was constructed to identify the interacting partners of DISC1. Based on the interaction scores, NDE1, GRM3, PTGER3 and KATNA1 were identified as functionally or physically related to DISC1, and may therefore regulate AD development. The DEPs were functionally annotated by Gene Ontology (GO) and Kyoto Encyclopedia of Genes and Genomes (KEGG) databases with the DAVID software, and the Non-supervised Orthologous Groups (eggNOG) database was used to determine their evolutionary relationships. The DEPs were significantly enriched in microtubules and mitochondria-related pathways. Gene set enrichment analysis (GSEA) was performed to identify genes and pathways that are activated when DISC1 is overexpressed. Our findings provide novel insights into the regulatory mechanisms underlying DISC1 function in AD.

Introduction

Alzheimer's disease (AD) is a highly prevalent neurodegenerative disease, and accounts for almost 80% of the dementia cases worldwide [1]. It commonly afflicts the elderly (>65 years), also known as the late-onset AD, and early-onset AD that affects those younger than 65 years of age is relatively rare [2]. It is characterized by the deposition of β-amyloid (Aβ) plaques and formation of neurofibrillary tangles (NFTs) of hyperphosphorylated tau protein, which impairs neuronal and synaptic functions [3–5].

Disrupted in Schizophrenia 1 (DISC1) is a multifunctional scaffold protein that is ubiquitous in the brain, and highly expressed in the temporal and para-hippocampal cortices, dentate gyrus of the hippocampus, and the white matter [6]. It interacts with multiple proteins involved in physiological processes such as neuron migration, neural progenitor cell (NPC) proliferation, neural signal transmission and synaptic functions, indicating a pathological role in neurodegeneration as well as a potential target for drug intervention [7]. Overexpression of DISC1 can reduce cognitive deficits and delay the progression of AD by protecting synaptic plasticity and down-regulating BACE1 [8,9]. However, the exact molecular mechanisms underlying the role of DISC1 in AD pathogenesis are unknown. To this end, we ectopically expressed DISC1 in the amyloid precursor protein (APP) cellular model of AD, and compared the proteomes of the control and overexpressing cells to identify the differentially expressed proteins (DEPs).

Received: 15 May 2021
Revised: 21 December 2021
Accepted: 23 December 2021

Accepted Manuscript online: 04 January 2022
Version of Record published: 11 January 2022

Bioscience Reports (2022) **42** BSR20211150
https://doi.org/10.1042/BSR20211150

Identifying proteins that interacted with DISC1 may reveal molecular mechanisms underlying DISC1 function in AD or other disorders.

Materials and methods

In vitro model of AD

The HEK293-APP cells were obtained from Institute of Neuroscience, Soochow University. The cells were transfected with the DISC1-overexpression (OE) and control lentiviruses (NC), and three replicates were used for each.

Protein extraction and digestion

Total protein was extracted from the cells using RIPA buffer (Beyotime, China) according to the manufacturer's protocol, and enzymatically digested with the filter-aided sample preparation (FASP) method [10]. Aliquots of lysates were mixed with 200 μl of 8 M urea in Nanosep Centrifugal Devices (PALL). The device was centrifuged at 14000×***g*** at 20°C for 20 min. All following centrifugation steps were performed applying the same conditions allowing maximal concentration. The concentrate was diluted with 200 μl of 8 M urea in 0.1 M Tris-HCl, pH 8.5 and the device was centrifuged. Proteins were reduced with 10 mM DTT for 2 h at 56°C. Subsequently, the samples were incubated in 5 mM iodoacetamide for 30 min in the dark to block reduced cysteine residues followed by centrifugation. The resulting concentrate was diluted with 200 μl of 8 M urea in 0.1 M Tris-HCl, pH 8.0 and concentrated again. This step was repeated two-times, and the concentrate was subjected to proteolytic digestion overnight at 37°C. The digests were collected by centrifugation, dried in a vacuum concentrator.

Isobaric tag for relative and absolute quantitation labeling

The tryptic digestion peptides were labeled with 8plex isobaric tag for relative and absolute quantitation (iTRAQ) reagents according to the manufacturer's instructions (Sciex, Foster City, CA). The dried peptides were resuspended in 200 mM triethylammonium bicarbonate (TEAB) buffer. For 50 μg peptide mixture per sample, half units of labeling reagent with respective isobaric tags from 113 to 119, which were dissolved in 140 μl isopropanol, were added into each sample tube, then vortexed for 1 min and incubated at room temperature for 2 h. The reaction was stopped with 100 μl high-performance liquid chromatography (HPLC) water for 30 min. The samples were labeled as (CON1)-113, (CON2)-114, (CON3)-115, (DISC1)-116, (DISC2)-117 and (DISC3)-118, (Mix)-119. Finally, all the samples were pooled and vacuum-dried for the next step.

Peptides fractionation by high pH reversed-phase liquid chromatography

Agilent 1100 HPLC system was used for peptides chromatographic fractionation. The dried sample was suspended in 110 μl solvent A (10 mM ammonium formate, 5% acetonitrile aqueous solution, pH = 10) and loaded on to an analytical C18 column (Zorbax Extended-C18, 2.1*150 mm, 5 μm, Agilent). A total of 80 min separation procedure was carried out at a flow rate of 300 μl/min with the monitoring wavelength of 215 nm, the elution gradient was set as follows: keep 5% solvent B (10 mM ammonium formate, 90% acetonitrile aqueous solution, pH = 10.0) for 5 min, increase from 5 to 38% solvent B in 60 min, from 38 to 90% B in 1 min, keep 90% B for 7 min, then equilibrate the column with 5% B for 7 min. A total of 48 fractions were evenly collected within the elution gradient starting from the 6 to 65th min, these 48 fractions were then pooled to generate the final 16 fractions using a nonadjacent pooling scheme (e.g., 1, 17, 49 pooled for final fraction 1; 2,18,50 pooled for final fraction 2). All the fractions were then dried in a vacuum for nano ESI-LC-MS/MS analysis.

Nano ESI-LC-MS/MS analysis

The lyophilized peptide fractions were resuspended in ddH_2O containing 0.1% formic acid, and 2 μl aliquots which were loaded into a nanoViper C18 (3 μm, 100 Å) trap column. The online chromatography seperation was performed on the Easy nLC 1200 system (Thermo Fisher). The trapping, desalting procedure were carried out with a volumn of 20 μl of 100% solvent A (0.1% formic acid). Then, an elution gradient of 8–38% solvent B (80% acetonitrile, 0.1% formic acid) at a flow rate of 300 nl/min (0–40 min, 5–38% B; 40–42 min, 38–100% B; 42–50 min, 100% B) in 60 min was used on an analytical column (50 μm × 15 cm C18-3 μm 100 Å). Data-dependent acquisition (DDA) mass spectrum techniques were used to acquire tandem MS data on a Thermo Fisher Q Exactive mass spectrometer (Thermo Fisher, U.S.A.) fitted with a Nano Flex ion source. Data were acquired using an ion spray voltage of 1.9 kV, and an interface heater temperature of 275°C. The mass spectrometry (MS) was operated with FULL-MS scans. For DDA, survey scans were acquired in 250 ms and up to 20 product ion scans (50 ms) were collected. Only spectra with a charge state of 2–4 were selected for fragmentation by higher energy collision energy. Dynamic exclusion was set for 25.

Identification analysis and quantitative analysis

The MS converter software (Version 1.3 beta Sciex) was used to convert the raw MS data into an open data format for subsequent analysis. Proteins were identified using the iPEAK tool that can combine results from multiple MS/MS search engines, including MSGFDB, X!tandem and MyriMatch [11]. The local false discovery rate (FDR) was 1% after searching against the amino acid sequences with a maximum of two missed cleavages and one missed termini cleavage (semitryptic digest). The following parameters were set for database searching: trypsin digestion, carbamidomethylation (C) of cysteine, iTRAQ8plex (N-term, K) as a fixed modification, and oxidation (M) and iTRAQ8plex (Y) as variable modifications. Precursor and fragment mass tolerance were set to 20 ppm and 0.05 Da, respectively. IQuant was used to quantify the labeled peptides with isobaric tags [12] using the following parameters: Quant_peptide of all unique peptides, Quant_number of at least one unique spectrum, variance stabilization normalization, Protein_Ratio of weighted average, and *t* test for Statistical Analysis. For protein abundance ratios, fold-changes ≥ 1.2 (or ≤ 0.833) and *P*-values <0.05 were the thresholds for statistical significance. The data were searched in the UniProt database using *Homo sapiens* (human) taxonomy (https://www.uniprot.org/proteomes/UP000005640).

Protein–protein interaction network construction

The STRING (version: 11.0b, https://string-db.org) search tool [13] was used to identify the key interacting proteins upstream and downstream of DISC1. Briefly, DEPs are imported into the database, and protein pairs with a total score > 0.4 were used to construct the protein–protein interaction (PPI) network that was further visualized by Cytoscape.

Gene Ontology, Kyoto Encyclopedia of Genes and Genomes and non-supervised Orthologous Groups analyses

Gene Ontology (GO), Kyoto Encyclopedia of Genes and Genomes (KEGG) and Non-supervised Orthologous Groups (eggNOG) analyses were performed using Bubble and Barplot Color Group tools in Hiplot basic model (https://hiplot.com.cn).

Enrichment statistical analysis of DEPs

The target genes and their associated functions were identified from GO database based on the biological process (BP), molecular function (MF) and cellular component (CC) categories. The various pathways involved in the DEPs were identified using the KEGG database. DAVID database tool (https://david.ncifcrf.gov/) [14,15] was used to identify the significantly enriched functions and pathways with $P<0.05$ as the threshold. The evolutionary genealogy of genes encoding for the DEPS was analyzed using the eggNOG [16] database with $P<0.05$ as statistically significant.

Gene set enrichment analysis

Gene set enrichment analysis (GSEA) was performed to screen for the gene sets and pathways enriched in the DISC1^{high} AD cells to identify genes associated with disease progression [17,18]. R clusterProfiler package [19] was used for GSEA on the basis of BP, MF, CC and KEGG categories. For each analysis, gene set permutations were implemented 5000 times. Gene sets with a FDR < 0.05 and adjusted *P*-value <0.05 were considered significantly enriched. The workflow of the study is outlined in Figure 1.

Results

DEPs screening and PPI network construction

Firstly, we detected the DISC1 expression level after overexpression of DISC1 in HEK-APP cells by Western blot. And we found DISC1 is up-regulated in HEK-APP cells compared with the control group (Supplementary Figure S1). Besides, according the results from our proteomics, DISC1 is overexpressed ∼2.18-folds than the control group. Then, a total of 351 DEPs (Supplementary Table S1) were identified in the DISC1^{high} AD cells relative to the control cells, and the top 20 up-regulated and down-regulated proteins are listed in Tables 1 and 2, respectively. The PPI network of the DEPs was then constructed using the STRING database to identify interacting partners (Figure 2A). As shown in Figure 2B, DISC1 directly or indirectly interacts with NDE1, GRM3, PTGER3 and KATNA1 at a physical and/or functional level.

Enrichment analysis of DEPs

The DEPs were functionally annotated with GO, KEGG and eggNOG enrichment analyses. As shown in Figure 3A, the DEPs were significantly enriched in transcription, mitochondrial promoter, intermediate filament cytoskeleton

Bioscience Reports (2022) **42** BSR20211150
https://doi.org/10.1042/BSR20211150

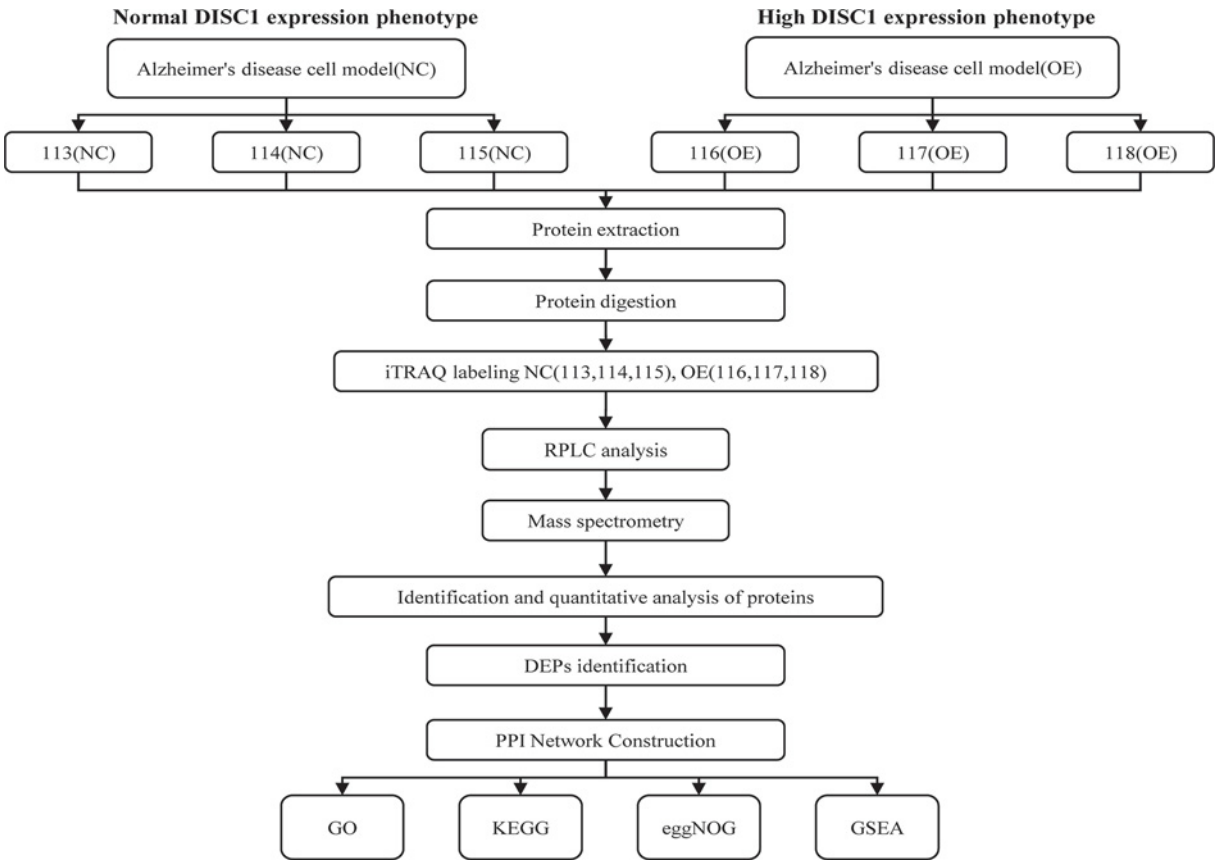

Figure 1. Schematic representation of the experimental design

Table 1 Top 20 up-regulated DEPs in AD cells overexpressing DISC1

Protein ID	Gene symbol	Description	Mean ratio
MRPL14	*PFN3*	Profilin-3	2.663172018
P62273	*RPS29*	40S ribosomal protein S29	2.481425328
Q9NRI5	*DISC1*	Disrupted in schizophrenia 1 protein	2.175152568
Q9UK76	*JPT1*	Jupiter microtubule-associated homolog 1	2.129304373
D6RIA3	*C4orf54*	Uncharacterized protein C4orf54	1.976621657
Q6P1L8	*MRPL14*	39S ribosomal protein L14, mitochondrial	1.946385443
Q71DI3	*HIST2H3A*	Histone H3.2	1.807106261
P05160	*F13B*	Coagulation factor XIII B chain	1.656737482
Q93077	*HIST1H2AC*	Histone H2A type 1-C	1.604556122
Q8WXG1	*RSAD2*	Radical S-adenosyl methionine domain-containing protein 2	1.593975355
P82921	*MRPS21*	28S ribosomal protein S21, mitochondrial	1.577483389
O75037	*KIF21B*	Kinesin-like protein KIF21B	1.570883653
Q9UK80	*USP21*	Ubiquitin carboxyl-terminal hydrolase 21	1.566709143
P52926	*HMGA2*	High mobility group protein HMGI-C	1.56653705
Q9BY77	*POLDIP3*	Polymerase δ-interacting protein 3	1.562567582
Q9Y6C2	*EMILIN1*	EMILIN-1	1.562523246
O00488	*ZNF593*	Zinc finger protein 593	1.561342328
Q9H446	*RWDD1*	RWD domain-containing protein 1	1.551293724
Q9NW61	*PLEKHJ1*	Pleckstrin homology domain-containing family J member 1	1.544695272
Q13442	*PDAP1*	28 kDa heat- and acid-stable phosphoprotein	1.542954482

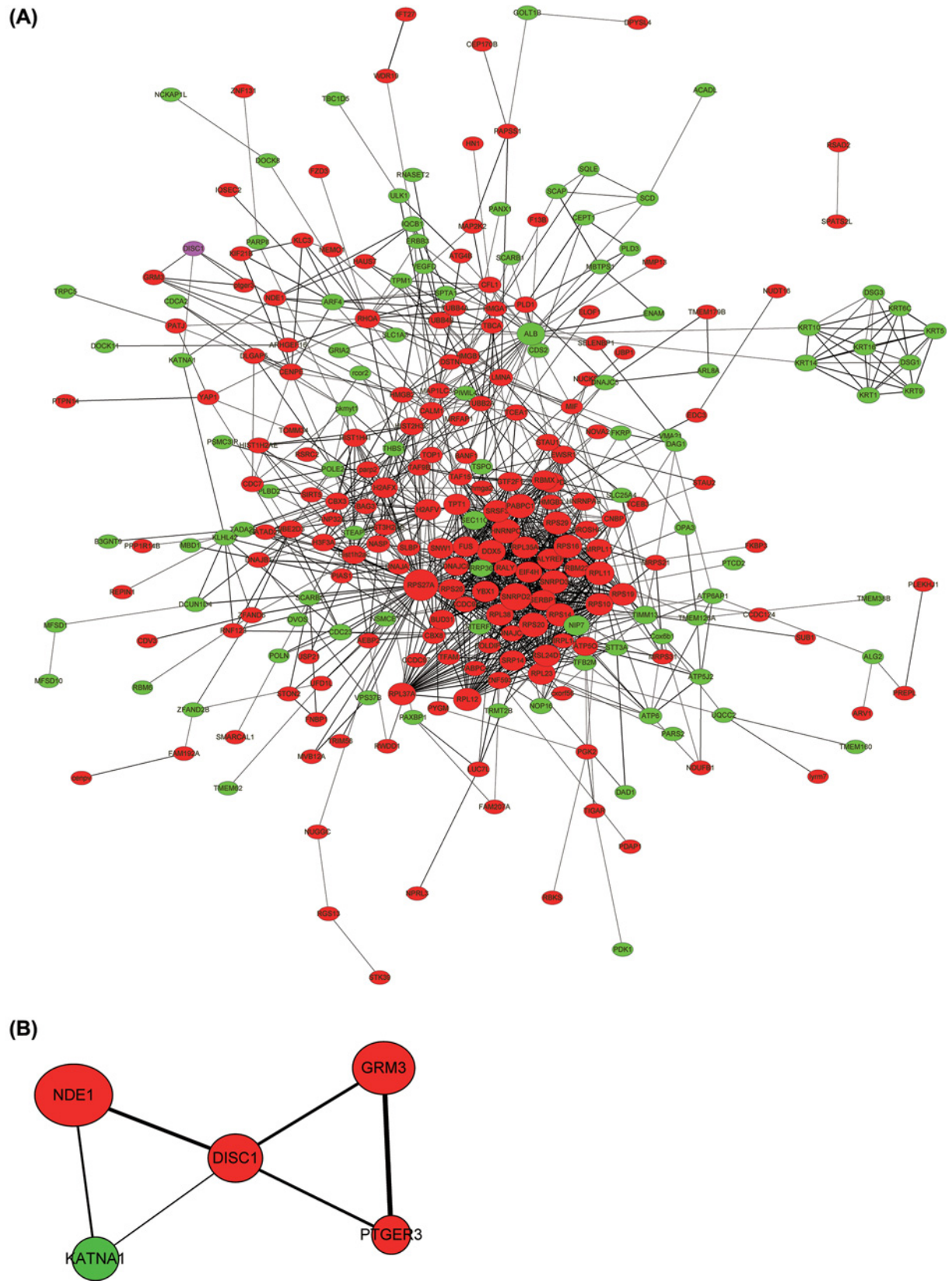

Figure 2. PPI network of DEPs

(**A**) The PPI network of DEPs was constructed by STRING and Cytoscape. Red nodes indicate up-regulated genes, green nodes indicate down-regulated genes. The node size correlates to the degree of connectivity and line thickness with interaction score. DISC1 is marked in purple in the upper left corner. (**B**) Proteins with physical or functional association with DISC1.

Bioscience Reports (2022) **42** BSR20211150
https://doi.org/10.1042/BSR20211150

Table 2 Top 20 down-regulated DEPs in AD cells overexpressing DISC1

Protein ID	Gene symbol	Description	Mean ratio
O95674	*CDS2*	Phosphatidate cytidylyltransferase 2	0.490415498
Q9H8M5	*CNNM2*	Metal transporter CNNM2	0.537252179
P78369	*CLDN10*	Claudin-10	0.553699125
Q9UL62	*TRPC5*	Short transient receptor potential channel 5	0.560397651
Q92858	*ATOH1*	Protein atonal homolog 1	0.561748688
P48668	*KRT6C*	Keratin, type II cytoskeletal 6C	0.56390028
P51786	*ZNF157*	Zinc finger protein 157	0.586087661
P13647	*KRT5*	Keratin, type II cytoskeletal 5	0.611197075
Q5HY64	*FAM47C*	Putative protein FAM47C	0.625502861
P08779	*KRT16*	Keratin, type I cytoskeletal 16	0.633121401
P21860	*ERBB3*	Receptor tyrosine-protein kinase erbB-3	0.643736939
P04264	*KRT1*	Keratin, type II cytoskeletal 1	0.656660409
P78332	*RBM6*	RNA-binding protein 6	0.656667186
Q96EU6	*RRP36*	Ribosomal RNA processing protein 36 homolog	0.680711277
Q9NX00	*TMEM160*	Transmembrane protein 160	0.685147795
Q92564	*DCUN1D4*	DCN1-like protein 4	0.691796699
Q9P003	*CNIH4*	Protein cornichon homolog 4	0.696978494
P80365	*HSD11B2*	Corticosteroid 11-beta-dehydrogenase isozyme 2	0.700629987
P28330	*ACADL*	Long-chain specific acyl-CoA dehydrogenase, mitochondrial	0.707497167
Q02413	*DSG1*	Desmoglein-1	0.707750707

organization, microtubule, mitochondrial inner membrane and mitochondrion etc. Furthermore, KEGG pathway analysis further showed that the ribosome, spliceosome, systemic lupus erythematosus, protein processing in the endoplasmic reticulum and Alcoholism pathways were significantly associated with the DEPs (Figure 3B) In additon, eggNOG enrichment analyses showed that posttranslational modification and translation were closely related to the DEPs (Figure 3C). The results are summarized in Table 3.

Identification of AD-related genes associated with DISC1

GSEA was performed to identify the AD-related gene sets in the DISC1^{high} AD cells. Significant differences were observed in the enriched GO terms and KEGG pathways of the DISC1^{low} and DISC1^{high} datasets. Microtubule-based process, microtubule cytoskeleton organization, mitochondrial transmembrane transport, transmembrane transport and oxidation–reduction were the significantly enriched BP categories in DISC1^{high} cells (Figure 4A), and the top five MF categories were cytoskeletal protein binding, calcium ion transmembrane transporter activity, heat shock protein (Hsp) binding, calcium ion binding and tubulin binding (Figure 4B). In addition, the DISC1^{high} phenotype showed significant enrichment of microtubule, cytoplasmic stress granule, microtubule-associated complex, kinesin complex and microtubule organizing center, along with a significant negative correlation with mitochondrial matrix, mitochondrial inner membrane component, inner mitochondrial membrane protein complex and mitochondrial protein complex (Figure 4C). Five REACTOME categories including nervous system development, post-chaperonin tubulin folding pathway, aggrephagy, Hsp90 chaperone cycle for steroid hormone receptors SHR, and the assembly and cell surface presentation of NMDA receptor were significantly enriched in the DISC1^{high} phenotype. While, mitochondrial protein import, respiratory electron transport ATP synthesis by chemiosmotic coupling and heat production by uncoupling proteins, and the citric acid TCA cycle and respiratory electron transport were negatively associated with this phenotype (Figure 4D). The results are summarized in Table 4.

Discussion

AD is the main cause of dementia and is a considerable socioeconomic burden worldwide [20]. The histological hallmarks of AD are extracellular accumulation of senile Aβ plaques, formation of intracellular NFTs, and glial cell-mediated inflammation [21,22]. However, the molecular mechanisms driving the pathophysiology of AD have

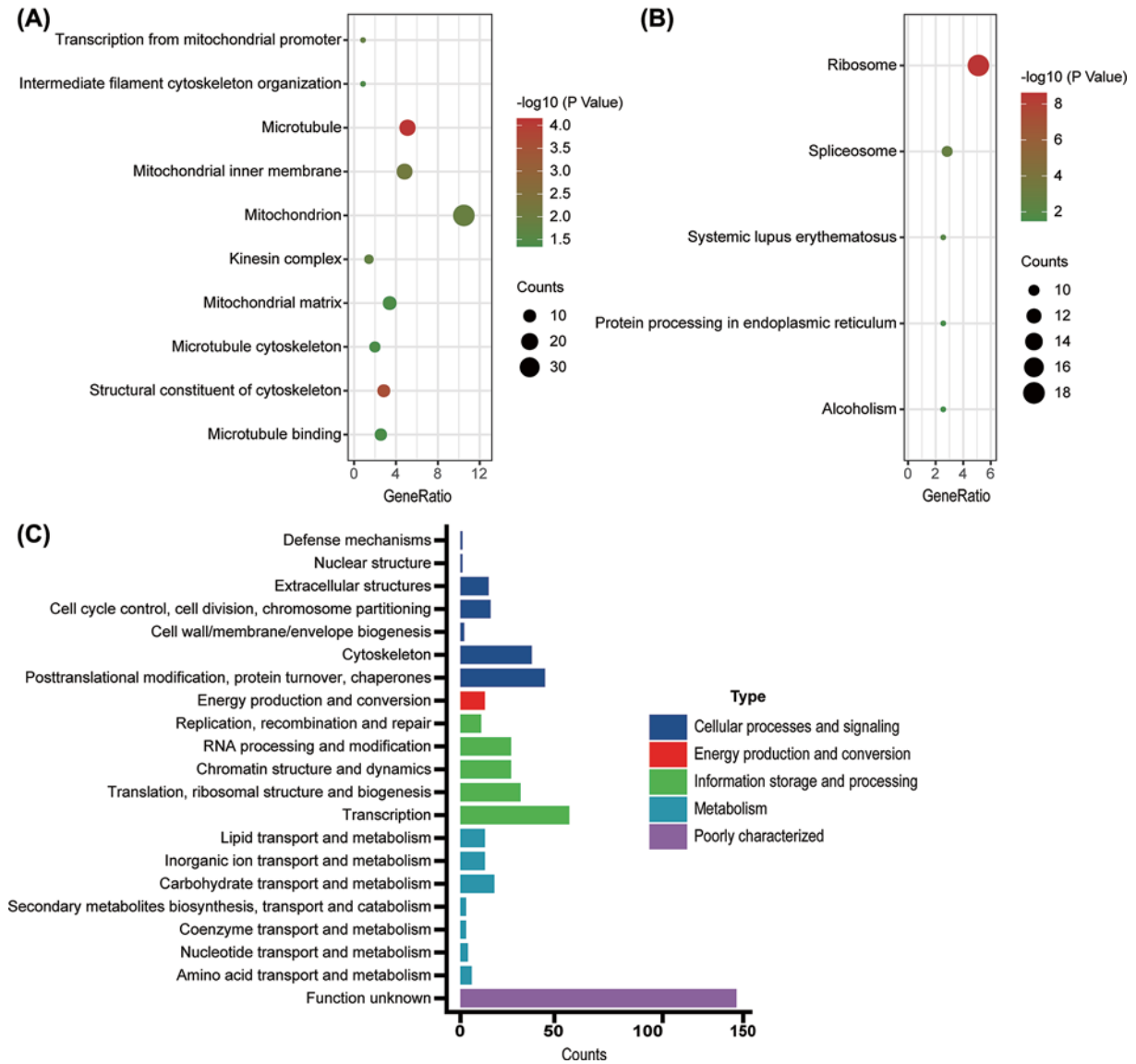

Figure 3. The enrichment analysis of DEPs

Functional enrichment analysis of GO (**A**). Functional enrichment analysis of KEGG (**B**). Functional enrichment analysis of eggNOG (**C**).

not completely elucidated. We previously showed that DISC1 slowed AD development by protecting synaptic plasticity and down-regulating BACE1 [8,9]. In the present study, we compared the proteomes of DISC1^{low} and DISC1^{high} AD cells to identify the proteins differentially expressed in response to DISC1 up-regulation. Through bioinformatics analysis, we identified key DSIC1-interacting proteins and pathways, mostly related to microtubules and mitochondria, that likely play important roles in the progression of AD.

Several studies have implicated microtubules in neurodegenerative diseases. Zempel et al. showed that the loss of microtubules is a risk factor in the progression of AD [23]. In our study, the DEPs and the gene sets correlated to DISC1 were significantly enriched in the microtubule and cytoskeleton-related functions and pathways. Furthermore, NDE1 and KATNA1, the proteins with high interaction score with DISC1, are involved in the microtubule and microtubule-binding pathways. Studies show that NDE1 is aberrantly expressed in neurological and psychiatric disorders [24,25], and binds to DISC1 to mediate the latter's role in neurogenesis and neural development [7,26]. In addition, KATNA1 regulates neuronal progenitor proliferation during embryonic development and adult neurogenesis

Bioscience Reports (2022) **42** BSR20211150
https://doi.org/10.1042/BSR20211150

Table 3 GO and KEGG pathway analyses of hub genes

Category	Term	Counts	GeneRatio	*P*-value
GOTERM_BP_DIRECT	GO:0006390~transcription from mitochondrial promoter	3	0.849858	0.014464
GOTERM_BP_DIRECT	GO:0045104~intermediate filament cytoskeleton organization	3	0.849858	0.031722
GOTERM_CC_DIRECT	GO:0005874~microtubule	18	5.09915	7.06E-05
GOTERM_CC_DIRECT	GO:0005743~mitochondrial inner membrane	17	4.815864	0.008035
GOTERM_CC_DIRECT	GO:0005739~mitochondrion	37	10.48159	0.013376
GOTERM_CC_DIRECT	GO:0005871~kinesin complex	5	1.416431	0.016361
GOTERM_CC_DIRECT	GO:0005759~mitochondrial matrix	12	3.399433	0.041063
GOTERM_CC_DIRECT	GO:0015630~microtubule cytoskeleton	7	1.983003	0.041571
GOTERM_MF_DIRECT	GO:0005200~structural constituent of cytoskeleton	10	2.832861	2.45E-04
GOTERM_MF_DIRECT	GO:0008017~microtubule binding	9	2.549575	0.045076
KEGG_PATHWAY	hsa03010:Ribosome	18	5.09915	2.44E-09
KEGG_PATHWAY	hsa03040:Spliceosome	10	2.832861	0.001809
KEGG_PATHWAY	hsa05322:Systemic lupus erythematosus	9	2.549575	0.006885
KEGG_PATHWAY	hsa04141:Protein processing in endoplasmic reticulum	9	2.549575	0.025116
KEGG_PATHWAY	hsa05034:Alcoholism	9	2.549575	0.031921

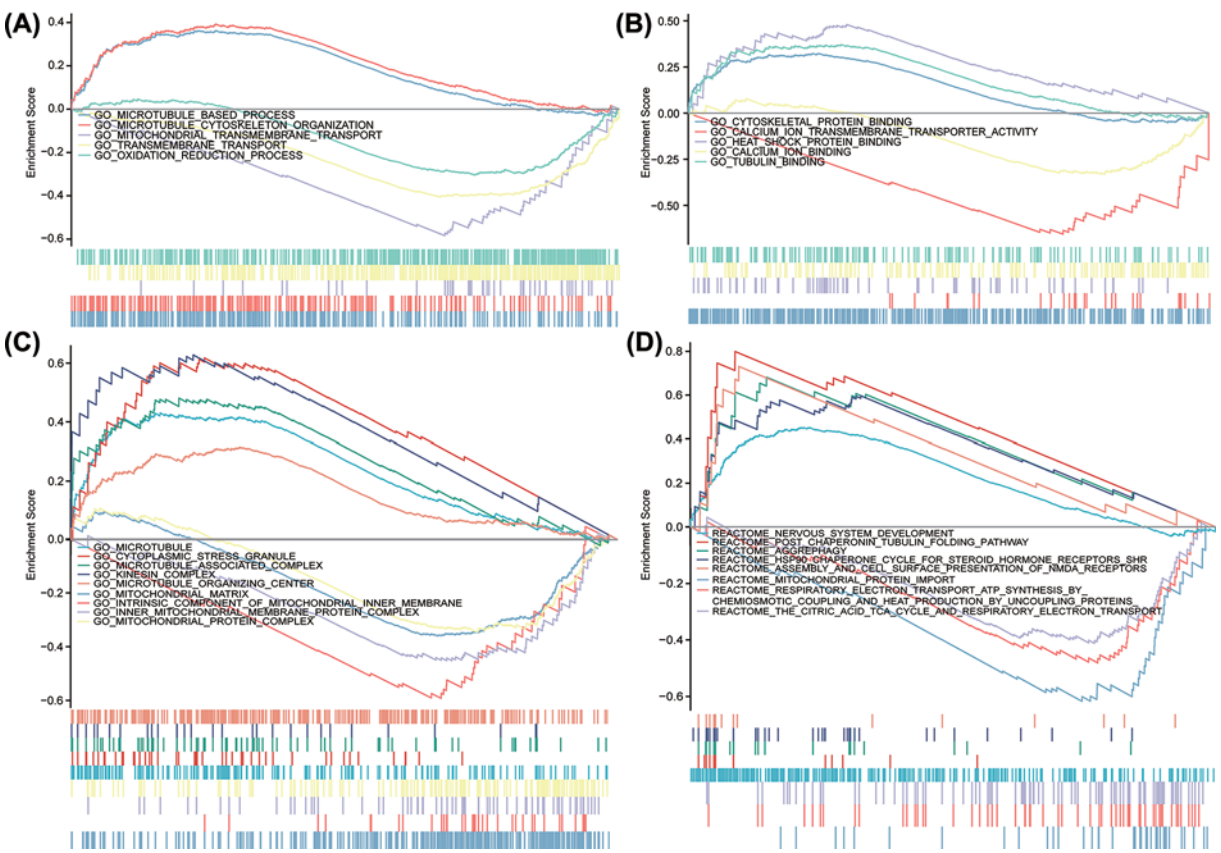

Figure 4. Enrichment plots from GSEA in DISC1^{high} phenotype

GSEA results showing DEPs in BP (**A**), MF (**B**), CC (**C**) and REACTOME (**D**). All results of GSEA were based on NES, adjusted *P*-value and FDR value.

Table 4 Gene sets enriched in high DISC1 expression phenotype

Gene set name	NES	*P*.adjust	FDR
BP			
GO_MICROTUBULE_BASED_PROCESS	1.619	0.032	0.03
GO_MICROTUBULE_CYTOSKELETON_ORGANIZATION	1.695	0.032	0.03
GO_MITOCHONDRIAL_TRANSMEMBRANE_TRANSPORT	−2.064	0.032	0.03
GO_TRANSMEMBRANE_TRANSPORT	−2.015	0.035	0.032
GO_OXIDATION_REDUCTION_PROCESS	−1.524	0.035	0.032
MF			
GO_CYTOSKELETAL_PROTEIN_BINDING	1.472	0.011	0.009
GO_CALCIUM_ION_TRANSMEMBRANE_TRANSPORTER _ACTIVITY	−2.085	0.011	0.009
GO_HEAT_SHOCK_PROTEIN_BINDING	1.748	0.031	0.025
GO_CALCIUM_ION_BINDING	−1.481	0.038	0.031
GO_TUBULIN_BINDING	1.533	0.047	0.038
CC			
GO_MICROTUBULE	1.813	0.011	0.009
GO_CYTOPLASMIC_STRESS_GRANULE	2.059	0.011	0.009
GO_MICROTUBULE_ASSOCIATED_COMPLEX	1.783	0.015	0.012
GO_KINESIN_COMPLEX	1.928	0.015	0.012
GO_MICROTUBULE_ORGANIZING_CENTER	1.401	0.049	0.04
GO_MITOCHONDRIAL_MATRIX	−1.754	0.014	0.011
GO_INTRINSIC_COMPONENT_OF_MITOCHONDRIAL_ INNER_MEMBRANE	−1.971	0.018	0.015
−GO_INNER_MITOCHONDRIAL_MEMBRANE_PROTEIN _COMPLEX	−1.725	0.018	0.015
GO_MITOCHONDRIAL_PROTEIN_COMPLEX	−1.548	0.026	0.021
REACTOME			
REACTOME_NERVOUS_SYSTEM_DEVELOPMENT	2.004	0.021	0.019
REACTOME_POST_CHAPERONIN_TUBULIN_FOLDING _PATHWAY	1.947	0.021	0.019
REACTOME_AGGREPHAGY	1.946	0.037	0.032
REACTOME_HSP90_CHAPERONE_CYCLE_FOR_ STEROID_HORMONE_RECEPTORS_SHR	1.89	0.045	0.04
REACTOME_ASSEMBLY_AND_CELL_SURFACE_ PRESENTATION_OF_NMDA_RECEPTORS	1.885	0.045	0.04
REACTOME_MITOCHONDRIAL_PROTEIN_IMPORT	−2.097	0.021	0.019
REACTOME_RESPIRATORY_ELECTRON_TRANSPORT_ATP_ SYNTHESIS_BY_CHEMIOSMOTIC_COUPLING_AND_ HEAT_PRODUCTION_BY_UNCOUPLING_PROTEINS	−1.782	0.045	0.04
REACTOME_THE_CITRIC_ACID_TCA_CYCLE_ AND_RESPIRATORY_ELECTRON_TRANSPORT	−1.676	0.048	0.042

Abbreviations: NES, normalized enrichment score; *P*.adjust, adjusted *P*-value.

[27]. Thus, DISC1 may directly or indirectly regulate NDE1 and KATNA1, and the downstream microtubule-related pathways to slow down the progression of AD.

The mitochondrial cascade hypothesis for AD was first proposed in 2004, and considers mitochondrial dysfunction as the prerequisite of events leading to AD [3]. Several studies have subsequently shown that mitochondrial dysfunction and oxidative stress play a central role in AD pathogenesis [28–31]. In our previous study, we reported that DISC1 functions as a mitophagy receptor that can clear the dysfunctional mitochondria [8]. In this study, we found that DEPs were significantly enriched in mitochondria-related functions and pathways. In addition, the negative NES values of these pathways in GSEA indicated that mitochondria-related functions are inhibited when DISC1 is highly expressed. Furthermore, cytoplasmic stress granule was an enriched CC category in GSEA, which is indicative of oxidative stress in the cytoplasm of AD cells. Therefore, DISC1 slows the progression of AD maybe by clearing the damaged mitochondria.

Pathways related to the kinesin complex, intracellular trafficking, vesicular transport and calcium influx were also enriched in the DEPs correlated to DISC1. Stokin et al. found that axonal lesions and defective microtubule-dependent transport are early pathological signs of AD, and that reduction in kinesin-I levels can increase Aβ generation and intraneuronal accumulation [32]. Besides, Murphy et al. demonstrated that the regulation of mitochondrial dynamics by DISC1, which is DISC1 robustly associates with mitochondrial trafficking on microtubule complexes, through multiple protein interaction, including DISC1, NDE1, kinesin complex etc., is a putative risk factor for major mental illness [33]. Furthermore, kinesin is also involved in the transport of mitochondria along axons, which is disrupted

Bioscience Reports (2022) **42** BSR20211150
https://doi.org/10.1042/BSR20211150

in neurodegenerative diseases [34–37]. Zempel et al. showed that calcium influx is also a significant factor in the pathogenesis of AD [23], which was validated by the enrichment of intracellular trafficking, secretion and vesicular transport by eggNOG analysis in our study. The pathways related to Hsp, aggrephagy and NMDAR were also enriched receptors among the DISC1-interacting proteins. Studies show that Hsp70 and Hsp90 can promote the clearance of Aβ plaques and delay the progression of AD [38–40]. Aggrephagy refers to the selective clearance of protein aggregates by autophagy [41]. The Aβ and tau aggregates are not effectively cleared due to dysfunctional aggrephagy, resulting in the formation of aggresomes that accelerate AD progression. Little is known regarding the mechanisms underlying aggrephagy, although there is evidence indicating that DISC1 can enhance this process [42]. Wang et al. found that the activation of synaptic NMDARs initiates plasticity and promotes neuronal survival, thereby slowing the progression of AD [43].

The other interacting partners of DISC1 identified by the PPI network were GRM3 and PTGER3 (interaction scores 0.630 and 0.627, respectively), which may also regulate DISC1 during AD progression. The GRM3 gene encodes mGluR3, which regulates neuronal and glial functions, as well as neuronal excitability and synaptic transmission [44]. Caraci et al. found that mGluR3 down-regulation and/or inactivation is correlated to impaired cognition in AD. The protective effect of mGluR3 against Aβ toxicity has also been observed in various animal models of AD, suggesting that age-related reduction in mGluR3 may contribute to the increased risk of AD [45]. Furthermore, Jin et al. found that postsynaptic mGluR3 strengthens working memory networks, and its inactivation erodes cognitive abilities [46]. PTGER3 is one of the four receptors of prostaglandin E2 (PGE2), a byproduct of arachidonic acid metabolism in the cyclooxygenase pathway, and is ubiquitously expressed in the brain [47,48]. Studies show that activation of PTGER3 can reduce or suppress cyclic adenosine monophosphate (cAMP) formation and may counteract its up-regulation via PTGER2, which has been linked to the anti-inflammatory effects of PGs. Altered PTGER3 expression in the microglia leads to acute or chronic microglial activation in brain diseases like AD [49].

In conclusion, DISC1 exerts a neuroprotective role during AD progression by interacting with NDE1, KATNA1, GRM3 and PTGER3, and regulating pathways related to microtubule function, mitochondrial dynamics, kinesin complex, calcium ion influx, Hsps, aggrephagy and NMDAR. Our findings will have to be verified by experimental studies. Nevertheless, the present study provides novel insights into the mechanisms driving AD progression, along with potential therapeutic targets that can revolutionize the individualized treatment of AD patients.

Data Availability

The datasets used and/or analyzed during the current study are available from the corresponding authors on reasonable request.

Competing Interests

The authors declare that there are no competing interests associated with the manuscript.

Funding

This work was supported by the National Natural Science Foundation of China [grant number 81901117]; the Natural Science Foundation of Guangdong Province [grant number 2019A1515010926]; the College Students' Science and Technology Innovation Project of Guangzhou Medical University [grant number 2020A024]; and the Health and Technology Project of Guangzhou [grant number 20211A010062].

CRediT Author Contribution

Jiajie Lu: Software, Writing—original draft. **Rihong Huang:** Data curation, Software. **Yuecheng Peng:** Software, Validation, Methodology. **Haojian Wang:** Investigation, Methodology. **Zejia Feng:** Investigation, Methodology. **Yongyang Fan:** Validation, Visualization, Methodology. **Zhaorong Zeng:** Validation, Visualization, Methodology. **Yezhong Wang:** Writing—original draft, Project administration, Writing—review & editing. **Jiana Wei:** Writing—original draft, Project administration, Writing—review & editing. **Zhaotao Wang:** Writing—original draft, Project administration, Writing—review & editing.

Abbreviations

AD, Alzheimer's disease; APP, amyloid precursor protein; Aβ, β-amyloid; BP, biological process; CC, cellular component; DDA, data-dependent acquisition; DEP, differentially expressed protein; DISC1, disrupted in schizophrenia 1; eggNOG, non-supervised Orthologous Groups; FDR, false discovery rate; GO, Gene Ontology; GSEA, gene set enrichment analysis; HPLC, high-performance liquid chromatography; Hsp, heat shock protein; iTRAQ, isobaric tag for relative and absolute quantitation; KEGG, Kyoto Encyclopedia of Genes and Genomes; MF, molecular function; MS, mass spectrometry; NFT, neurofibrillary tangle; PPI, protein–protein interaction.

References

1 Alzheimer's Association (2020) Alzheimer's disease facts and figures. *Alzheimers Dement.*, https://doi.org/10.1002/alz.12068
2 Van Cauwenberghe, C., Van Broeckhoven, C. and Sleegers, K. (2016) The genetic landscape of Alzheimer disease: clinical implications and perspectives. *Genet. Med.* **18**, 421–430, https://doi.org/10.1038/gim.2015.117
3 Swerdlow, R.H. and Khan, S.M. (2004) A "mitochondrial cascade hypothesis" for sporadic Alzheimer's disease. *Med. Hypotheses* **63**, 8–20, https://doi.org/10.1016/j.mehy.2003.12.045
4 Swerdlow, R.H., Burns, J.M. and Khan, S.M. (2014) The Alzheimer's disease mitochondrial cascade hypothesis: progress and perspectives. *Biochim. Biophys. Acta* **1842**, 1219–1231, https://doi.org/10.1016/j.bbadis.2013.09.010
5 Yao, J., Irwin, R.W., Zhao, L. et al. (2009) Mitochondrial bioenergetic deficit precedes Alzheimer's pathology in female mouse model of Alzheimer's disease. *Proc. Natl. Acad. Sci. U.S.A.* **106**, 14670–14675, https://doi.org/10.1073/pnas.0903563106
6 Lipska, B.K., Peters, T., Hyde, T.M. et al. (2006) Expression of disc1 binding partners is reduced in schizophrenia and associated with disc1 snps. *Hum. Mol. Genet.* **15**, 1245–1258, https://doi.org/10.1093/hmg/ddl040
7 Bradshaw, N.J. and Porteous, D.J. (2012) Disc1-binding proteins in neural development, signalling and schizophrenia. *Neuropharmacology* **62**, 1230–1241, https://doi.org/10.1016/j.neuropharm.2010.12.027
8 Wang, Z.T., Lu, M.H., Zhang, Y. et al. (2019) Disrupted-in-schizophrenia-1 protects synaptic plasticity in a transgenic mouse model of Alzheimer's disease as a mitophagy receptor. *Aging Cell* **18**, e12860, https://doi.org/10.1111/acel.12860
9 Deng, Q.S., Dong, X.Y., Wu, H. et al. (2016) Disrupted-in-schizophrenia-1 attenuates amyloid-β generation and cognitive deficits in app/ps1 transgenic mice by reduction of β-site app-cleaving enzyme 1 levels. *Neuropsychopharmacology* **41**, 440–453, https://doi.org/10.1038/npp.2015.164
10 Wisniewski, J.R., Zougman, A., Nagaraj, N. et al. (2009) Universal sample preparation method for proteome analysis. *Nat. Methods* **6**, 359–362, https://doi.org/10.1038/nmeth.1322
11 Wen, B., Du, C., Li, G. et al. (2015) Ipeak: an open source tool to combine results from multiple ms/ms search engines. *Proteomics* **15**, 2916–2920, https://doi.org/10.1002/pmic.201400208
12 Wen, B., Zhou, R., Feng, Q. et al. (2014) Iquant: an automated pipeline for quantitative proteomics based upon isobaric tags. *Proteomics* **14**, 2280–2285, https://doi.org/10.1002/pmic.201300361
13 Szklarczyk, D., Gable, A.L., Lyon, D. et al. (2019) String v11: protein-protein association networks with increased coverage, supporting functional discovery in genome-wide experimental datasets. *Nucleic Acids Res.* **47**, D607–D613, https://doi.org/10.1093/nar/gky1131
14 Huang, D.W., Sherman, B. and Lempicki, R.J. (2009) Systematic and integrative analysis of large gene lists using david bioinformatics resources. *Nat. Protoc.* **4**, 44–57, https://doi.org/10.1038/nprot.2008.211
15 Huang, D.W., Sherman, B. and Lempicki, R.J. (2009) Bioinformatics enrichment tools: Paths toward the comprehensive functional analysis of large gene lists. *Nucleic Acids Res.* **37**, 1–13, https://doi.org/10.1093/nar/gkn923
16 Huerta-Cepas, J., Szklarczyk, D., Forslund, K. et al. (2016) Eggnog 4.5: A hierarchical orthology framework with improved functional annotations for eukaryotic, prokaryotic and viral sequences. *Nucleic Acids Res.* **44**, D286–D293, https://doi.org/10.1093/nar/gkv1248
17 Subramanian, A., Kuehn, H., Gould, J. et al. (2007) Gsea-p: a desktop application for gene set enrichment analysis. *Bioinformatics* **23**, 3251–3253, https://doi.org/10.1093/bioinformatics/btm369
18 Subramanian, A., Tamayo, P., Mootha, V. et al. (2005) Gene set enrichment analysis: a knowledge-based approach for interpreting genome-wide expression profiles. *Proc. Natl. Acad. Sci. U.S.A.* **102**, 15545–15550, https://doi.org/10.1073/pnas.0506580102
19 Yu, G., Wang, L., Han, Y. et al. (2012) Clusterprofiler: an r package for comparing biological themes among gene clusters. *OMICS* **16**, 284–287, https://doi.org/10.1089/omi.2011.0118
20 Europe, A. (2020) Dementia in Europe yearbook 2019: estimating the prevalence of dementia in Europe. https://www.alzheimereurope.org/content/download/195515/1457520/file/FINAL%2005707%20Alzheimer%20Europe%20yearbook%202019.pdf
21 Selkoe, D.J. and Schenk, D. (2003) Alzheimer's disease: molecular understanding predicts amyloid-based therapeutics. *Annu. Rev. Pharmacol. Toxicol.* **43**, 545–584, https://doi.org/10.1146/annurev.pharmtox.43.100901.140248
22 Kuhlmann, J., Andreasson, U., Pannee, J. et al. (2017) Csf aβ(1-42) - an excellent but complicated alzheimer's biomarker - a route to standardisation. *Clin. Chim. Acta* **467**, 27–33, https://doi.org/10.1016/j.cca.2016.05.014
23 Zempel, H. and Mandelkow, E.-M. (2012) Linking amyloid-β and tau: Amyloid-β induced synaptic dysfunction via local wreckage of the neuronal cytoskeleton. *Neurodegener. Dis.* **10**, 64–72, https://doi.org/10.1159/000332816
24 Bradshaw, N.J. and Hayashi, M.A. (2017) Nde1 and ndel1 from genes to (mal)functions: parallel but distinct roles impacting on neurodevelopmental disorders and psychiatric illness. *Cell. Mol. Life Sci.* **74**, 1191–1210, https://doi.org/10.1007/s00018-016-2395-7
25 Pei, Z., Lang, B., Fragoso, Y.D. et al. (2014) The expression and roles of nde1 and ndel1 in the adult mammalian central nervous system. *Neuroscience* **271**, 119–136, https://doi.org/10.1016/j.neuroscience.2014.04.031
26 Ye, F., Kang, E., Yu, C. et al. (2017) Disc1 regulates neurogenesis via modulating kinetochore attachment of ndel1/nde1 during mitosis. *Neuron* **96**, 1041–1054 e5, https://doi.org/10.1016/j.neuron.2017.11.034
27 Lombino, F., Muhia, M., Lopez-Rojas, J. et al. (2019) The microtubule severing protein katanin regulates proliferation of neuronal progenitors in embryonic and adult neurogenesis. *Sci. Rep.* **9**, 15940, https://doi.org/10.1038/s41598-019-52367-3
28 Dai, C., Luo, T., Luo, S. et al. (2016) P53 and mitochondrial dysfunction: novel insight of neurodegenerative diseases. *J. Bioenerg. Biomembr.* **48**, 337–347, https://doi.org/10.1007/s10863-016-9669-5
29 Chen, H. and Chan, D.J. (2009) Mitochondrial dynamics–fusion, fission, movement, and mitophagy–in neurodegenerative diseases. *Hum. Mol. Genet.* **18**, R169–R176, https://doi.org/10.1093/hmg/ddp326

30 Cha, M., Han, S., Son, S. et al. (2012) Mitochondria-specific accumulation of amyloid β induces mitochondrial dysfunction leading to apoptotic cell death. *PLoS ONE* **7**, e34929, https://doi.org/10.1371/journal.pone.0034929
31 Maruszak, A. and Zekanowski, C. (2011) Mitochondrial dysfunction and Alzheimer's disease. *Prog. Neuropsychopharmacol. Biol. Psychiatry* **35**, 320–330, https://doi.org/10.1016/j.pnpbp.2010.07.004
32 Stokin, G.B., Lillo, C., Falzone, T.L. et al. (2005) Axonopathy and transport deficits early in the pathogenesis of alzheimer's disease. *Science* **307**, 1282–1288, https://doi.org/10.1126/science.1105681
33 Murphy, L.C. and Millar, J.K. (2017) Regulation of mitochondrial dynamics by disc1, a putative risk factor for major mental illness. *Schizophr. Res.* **187**, 55–61, https://doi.org/10.1016/j.schres.2016.12.027
34 Chen, Y. and Sheng, Z.J.T. (2013) Kinesin-1-syntaphilin coupling mediates activity-dependent regulation of axonal mitochondrial transport. *J. Cell Biol.* **202**, 351–364, https://doi.org/10.1083/jcb.201302040
35 Chaturvedi, R. and Flint Beal, M. (2013) Mitochondrial diseases of the brain. *Free Radic. Biol. Med.* **63**, 1–29, https://doi.org/10.1016/j.freeradbiomed.2013.03.018
36 Brickley, K. and Stephenson, F. (2011) Trafficking kinesin protein (trak)-mediated transport of mitochondria in axons of hippocampal neurons. *J. Biol. Chem.* **286**, 18079–18092, https://doi.org/10.1074/jbc.M111.236018
37 Chen, H. and Chan, D.C. (2009) Mitochondrial dynamics–fusion, fission, movement, and mitophagy–in neurodegenerative diseases. *Hum. Mol. Genet.* **18**, R169–R176, https://doi.org/10.1093/hmg/ddp326
38 Magrané, J., Smith, R., Walsh, K. et al. (2004) Heat shock protein 70 participates in the neuroprotective response to intracellularly expressed beta-amyloid in neurons. *J. Neurosci.* **24**, 1700–1706
39 Kakimura, J., Kitamura, Y., Takata, K. et al. (2002) Microglial activation and amyloid-beta clearance induced by exogenous heat-shock proteins. *FASEB J.* **16**, 601–603, https://doi.org/10.1096/fj.01-0530fje
40 Hoshino, T., Murao, N., Namba, T. et al. (2011) Suppression of Alzheimer's disease-related phenotypes by expression of heat shock protein 70 in mice. *J. Neurosci.* **31**, 5225–5234, https://doi.org/10.1523/JNEUROSCI.5478-10.2011
41 Øverbye, A., Fengsrud, M. and Seglen, P. (2007) Proteomic analysis of membrane-associated proteins from rat liver autophagosomes. *Autophagy* **3**, 300–322, https://doi.org/10.4161/auto.3910
42 Malampati, S., Song, J.X., Chun-Kit Tong, B. et al. (2020) Targeting aggrephagy for the treatment of Alzheimer's disease. *Cells* **9**, 311, https://doi.org/10.3390/cells9020311
43 Wang, R. and Reddy, P.H. (2017) Role of glutamate and nmda receptors in Alzheimer's disease. *J. Alzheimers Dis.* **57**, 1041–1048, https://doi.org/10.3233/JAD-160763
44 Niswender, C.M. and Conn, P.J. (2010) Metabotropic glutamate receptors: Physiology, pharmacology, and disease. *Annu. Rev. Pharmacol. Toxicol.* **50**, 295–322, https://doi.org/10.1146/annurev.pharmtox.011008.145533
45 Caraci, F., Molinaro, G., Battaglia, G. et al. (2011) Targeting group ii metabotropic glutamate (mglu) receptors for the treatment of psychosis associated with Alzheimer's disease: selective activation of mglu2 receptors amplifies beta-amyloid toxicity in cultured neurons, whereas dual activation of mglu2 and mglu3 receptors is neuroprotective. *Mol. Pharmacol.* **79**, 618–626, https://doi.org/10.1124/mol.110.067488
46 Jin, L.E., Wang, M., Galvin, V.C. et al. (2018) Mglur2 versus mglur3 metabotropic glutamate receptors in primate dorsolateral prefrontal cortex: postsynaptic mglur3 strengthen working memory networks. *Cereb. Cortex* **28**, 974–987, https://doi.org/10.1093/cercor/bhx005
47 Nakamura, K., Kaneko, T., Yamashita, Y. et al. (2000) Immunohistochemical localization of prostaglandin ep3 receptor in the rat nervous system. *J. Comp. Neurol.* **421**, 543–569, https://doi.org/10.1002/(SICI)1096-9861(20000612)421:4%3c543::AID-CNE6%3e3.0.CO;2-3
48 Narumiya, S., Sugimoto, Y. and Ushikubi, F. (1999) Prostanoid receptors: structures, properties, and functions. *Physiol. Rev.* **79**, 1193–1226, https://doi.org/10.1152/physrev.1999.79.4.1193
49 Slawik, H., Volk, B., Fiebich, B. et al. (2004) Microglial expression of prostaglandin ep3 receptor in excitotoxic lesions in the rat striatum. *Neurochem. Int.* **45**, 653–660, https://doi.org/10.1016/j.neuint.2004.04.007

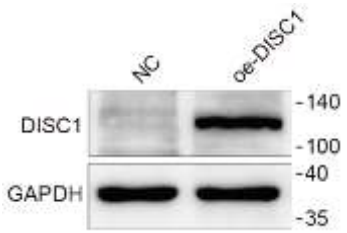

Supplementary Figure. S1

Western blot analysis of levels of DISC1protein in HEK293-APP cells which were transfected with DISC1-overexpression (OE) or control lentiviruses (vector).

Supplementary Table. S1 351 DEPs in model cells of AD over-expressing DISC1.

Protein ID	Gene symbol	Description	Mean ratio
P60673	PFN3	Profilin-3	2.663172018
P62273	RPS29	40S ribosomal protein S29	2.481425328
Q9NRI5	DISC1	Disrupted in schizophrenia 1 protein	2.175152568
Q9UK76	JPT1	Jupiter microtubule associated homolog 1	2.129304373
D6RIA3	C4orf54	Uncharacterized protein C4orf54	1.976621657
Q6P1L8	MRPL14	39S ribosomal protein L14, mitochondrial	1.946385443
Q71DI3	HIST2H3A	Histone H3.2	1.807106261
P05160	F13B	Coagulation factor XIII B chain	1.656737482
Q93077	HIST1H2AC	Histone H2A type 1-C	1.604556122
Q8WXG1	RSAD2	Radical S-adenosyl methionine domain-containing protein 2	1.593975355
P82921	MRPS21	28S ribosomal protein S21, mitochondrial	1.577483389
O75037	KIF21B	Kinesin-like protein KIF21B	1.570883653
Q9UK80	USP21	Ubiquitin carboxyl-terminal hydrolase 21	1.566709143
P52926	HMGA2	High mobility group protein HMGI-C	1.56653705
Q9BY77	POLDIP3	Polymerase delta-interacting protein 3	1.562567582
Q9Y6C2	EMILIN1	EMILIN-1	1.562523246
O00488	ZNF593	Zinc finger protein 593	1.561342328
Q9H446	RWDD1	RWD domain-containing protein 1	1.551293724
Q9NW61	PLEKHJ1	Pleckstrin homology domain-containing family J member 1	1.544695272
Q13442	PDAP1	28 kDa heat- and acid-stable phosphoprotein	1.542954482
O95793	STAU1	Double-stranded RNA-binding protein Staufen homolog 1	1.52148379
O14921	RGS13	Regulator of G-protein signaling 13	1.518755395
P35637	FUS	RNA-binding protein FUS	1.51176635
Q8WXE9	STON2	Stonin-2	1.510145096
P04908	HIST1H2AB	Histone H2A type 1-B/E	1.499748278
Q9NZC9	SMARCAL1	SWI/SNF-related matrix-associated actin-dependent regulator of chromatin subfamily A-like protein 1	1.484634212
P60866	RPS20	40S ribosomal protein S20	1.471888769
P62913	RPL11	60S ribosomal protein L11	1.469239167
O00311	CDC7	Cell division cycle 7-related protein kinase	1.459651794
Q99871	HAUS7	HAUS augmin-like complex subunit 7	1.452152209
Q5VWW1	C1QL3	Complement C1q-like protein 3	1.429847408
P84103	SRSF3	Serine/arginine-rich splicing factor 3	1.425031204
P09429	HMGB1	High mobility group protein B1	1.421077504
P41223	BUD31	Protein BUD31 homolog	1.417104628
Q9NZP6	NPAP1	Nuclear pore-associated protein 1	1.405854464
Q02224	CENPE	Centromere-associated protein E	1.391536488
Q5XPI4	RNF123	E3 ubiquitin-protein ligase RNF123	1.38593246
Q9H492	MAP1LC3A	Microtubule-associated proteins 1A/1B light	1.384994248

		chain 3A	
Q9UKM9	RALY	RNA-binding protein Raly	1.379526179
Q96DE0	NUDT16	U8 snoRNA-decapping enzyme	1.378987515
Q6FIF0	ZFAND6	AN1-type zinc finger protein 6	1.377644089
Q71UI9	H2AFV	Histone H2A.V	1.367391837
P62263	RPS14	40S ribosomal protein S14	1.364455781
Q9UNW9	NOVA2	RNA-binding protein Nova-2	1.361265134
P62633	CNBP	Cellular nucleic acid-binding protein	1.358100889
P38159	RBMX	RNA-binding motif protein, X chromosome	1.358088598
P84243	H3F3A	Histone H3.3	1.357848195
P25685	DNAJB1	DnaJ homolog subfamily B member 1	1.357253446
P60002	ELOF1	Transcription elongation factor 1 homolog	1.357118803
P62316	SNRPD2	Small nuclear ribonucleoprotein Sm D2	1.350704621
Q9NUL3	STAU2	Double-stranded RNA-binding protein Staufen homolog 2	1.350569347
P45452	MMP13	Collagenase 3	1.348205049
P26583	HMGB2	High mobility group protein B2	1.347960919
Q14493	SLBP	Histone RNA hairpin-binding protein	1.339336978
P62805	HIST1H4A	Histone H4	1.338675082
P60981	DSTN	Destrin	1.338360807
Q14832	GRM3	Metabotropic glutamate receptor 3	1.337731441
Q9NW64	RBM22	Pre-mRNA-splicing factor RBM22	1.33489686
P30050	RPL12	60S ribosomal protein L12	1.327390437
Q86TN4	TRPT1	tRNA 2'-phosphotransferase 1	1.32606524
Q9NXW9	ALKBH4	Alpha-ketoglutarate-dependent dioxygenase alkB homolog 4	1.325937978
Q9NPG1	FZD3	Frizzled-3	1.322624257
O75925	PIAS1	E3 SUMO-protein ligase PIAS1	1.321503766
Q01844	EWSR1	RNA-binding protein EWS	1.319601261
Q53QV2	LBH	Protein LBH	1.318861536
O75531	BANF1	Barrier-to-autointegration factor	1.314593528
Q00688	FKBP3	Peptidyl-prolyl cis-trans isomerase FKBP3	1.313956247
Q6NXN4	DPY19L2P1	Putative C-mannosyltransferase DPY19L2P1	1.310855929
Q9H8W4	PLEKHF2	Pleckstrin homology domain-containing family F member 2	1.309976401
P61077	UBE2D3	Ubiquitin-conjugating enzyme E2 D3	1.305305759
Q13393	PLD1	Phospholipase D1	1.304721135
O14531	DPYSL4	Dihydropyrimidinase-related protein 4	1.304654158
Q9HC52	CBX8	Chromobox protein homolog 8	1.304094296
Q8NH81	OR10G6	Olfactory receptor 10G6	1.30345953
Q9HBM6	TAF9B	Transcription initiation factor TFIID subunit 9B	1.302202026
Q9NZP5	OR5AC2	Olfactory receptor 5AC2	1.298908529
Q96EK6	GNPNAT1	Glucosamine 6-phosphate N-acetyltransferase	1.297054425
P17096	HMGA1	High mobility group protein HMG-I/HMG-Y	1.290807567
Q9NRR4	DROSHA	Ribonuclease 3	1.290265936
O15061	SYNM	Synemin	1.289195829
Q9NXR1	NDE1	Nuclear distribution protein nudE homolog 1	1.288709326

P11940	PABPC1	Polyadenylate-binding protein 1	1.285071017
Q7Z7K6	CENPV	Centromere protein V	1.283916595
Q68CJ6	NUGGC	Nuclear GTPase SLIP-GC	1.283641361
P18077	RPL35A	60S ribosomal protein L35a	1.283026404
Q96CT7	CCDC124	Coiled-coil domain-containing protein 124	1.281811492
P62318	SNRPD3	Small nuclear ribonucleoprotein Sm D3	1.281563466
Q96F86	EDC3	Enhancer of mRNA-decapping protein 3	1.280314048
Q5VV41	ARHGEF16	Rho guanine nucleotide exchange factor 16	1.279495682
Q9UN81	L1RE1	LINE-1 retrotransposable element ORF1 protein	1.279078071
O75937	DNAJC8	DnaJ homolog subfamily C member 8	1.275320043
P61513	RPL37A	60S ribosomal protein L37a	1.27469655
Q96N11	C7orf26	Uncharacterized protein C7orf26	1.272927269
P23193	TCEA1	Transcription elongation factor A protein 1	1.266354628
Q9UGN5	PARP2	Poly [ADP-ribose] polymerase 2	1.263690485
P68371	TUBB4B	Tubulin beta-4B chain	1.263359478
Q99729	HNRNPAB	Heterogeneous nuclear ribonucleoprotein A/B	1.261724378
Q4J6C6	PREPL	Prolyl endopeptidase-like	1.261697724
Q96EY5	MVB12A	Multivesicular body subunit 12A	1.261182618
Q9BRZ2	TRIM56	E3 ubiquitin-protein ligase TRIM56	1.260905818
Q8IYE0	CCDC146	Coiled-coil domain-containing protein 146	1.260509627
Q9H2C2	ARV1	Protein ARV1	1.260370968
Q562E7	WDR81	WD repeat-containing protein 81	1.260227986
Q9H477	RBKS	Ribokinase	1.260169904
O15347	HMGB3	High mobility group protein B3	1.258228304
Q9BWE0	REPIN1	Replication initiator 1	1.257249586
P46783	RPS10	40S ribosomal protein S10	1.256715091
Q12980	NPRL3	GATOR complex protein NPRL3	1.255275227
Q9Y3S2	ZNF330	Zinc finger protein 330	1.254775718
Q9NZI7	UBP1	Upstream-binding protein 1	1.254692752
Q9NXA8	SIRT5	NAD-dependent protein deacylase sirtuin-5, mitochondrial	1.253462074
P07910	HNRNPC	Heterogeneous nuclear ribonucleoproteins C1/C2	1.253406773
Q8N653	LZTR1	Leucine-zipper-like transcriptional regulator 1	1.253380617
Q7Z7N9	TMEM179B	Transmembrane protein 179B	1.253120454
P36507	MAP2K2	Dual specificity mitogen-activated protein kinase kinase 2	1.252605327
Q13268	DHRS2	Dehydrogenase/reductase SDR family member 2, mitochondrial	1.251813455
P53999	SUB1	Activated RNA polymerase II transcriptional coactivator p15	1.248839311
Q9H1E3	NUCKS1	Nuclear ubiquitous casein and cyclin-dependent kinase substrate 1	1.248676421
Q9H788	SH2D4A	SH2 domain-containing protein 4A	1.247815744
Q8IWC1	MAP7D3	MAP7 domain-containing protein 3	1.247372034
P43115	PTGER3	Prostaglandin E2 receptor EP3 subtype	1.246879059
Q6ZN18	AEBP2	Zinc finger protein AEBP2	1.24648453
Q8NI35	PATJ	InaD-like protein	1.24623144
Q9Y4F5	CEP170B	Centrosomal protein of 170 kDa protein B	1.245492435

Q8N128	FAM177A1	Protein FAM177A1	1.245199779
Q7L4I2	RSRC2	Arginine/serine-rich coiled-coil protein 2	1.244248862
P07205	PGK2	Phosphoglycerate kinase 2	1.243494777
Q13573	SNW1	SNW domain-containing protein 1	1.242602105
Q15678	PTPN14	Tyrosine-protein phosphatase non-receptor type 14	1.241718451
Q9Y316	MEMO1	Protein MEMO1	1.241687677
Q15398	DLGAP5	Disks large-associated protein 5	1.241359914
P29373	CRABP2	Cellular retinoic acid-binding protein 2	1.239320246
Q9BW85	YJU2	YJU2 splicing factor homolog	1.238269443
P48047	ATP5O	ATP synthase subunit O, mitochondrial	1.23680797
P46937	YAP1	Transcriptional coactivator YAP1	1.236755164
Q8TF05	PPP4R1	Serine/threonine-protein phosphatase 4 regulatory subunit 1	1.235827235
P14174	MIF	Macrophage migration inhibitory factor	1.235406376
Q86YP4	GATAD2A	Transcriptional repressor p66-alpha	1.234582282
Q86V81	ALYREF	THO complex subunit 4	1.234053994
P23528	CFL1	Cofilin-1	1.233962302
Q9NQ88	TIGAR	Fructose-2,6-bisphosphatase TIGAR	1.233681399
P62249	RPS16	40S ribosomal protein S16	1.233594379
Q8N257	HIST3H2BB	Histone H2B type 3-B	1.23305659
Q9BSD7	NTPCR	Cancer-related nucleoside-triphosphatase	1.232872203
Q00059	TFAM	Transcription factor A, mitochondrial	1.232248125
Q16775	HAGH	Hydroxyacylglutathione hydrolase, mitochondrial	1.231666132
Q9UKY7	CDV3	Protein CDV3 homolog	1.23165581
Q15785	TOMM34	Mitochondrial import receptor subunit TOM34	1.230957984
Q5JU85	IQSEC2	IQ motif and SEC7 domain-containing protein 2	1.229717616
Q9NUQ6	SPATS2L	SPATS2-like protein	1.229699318
P13693	TPT1	Translationally-controlled tumor protein	1.228899859
Q9BW83	IFT27	Intraflagellar transport protein 27 homolog	1.227714854
Q9NSI2	FAM207A	Protein FAM207A	1.226779957
O75347	TBCA	Tubulin-specific chaperone A	1.225323104
Q9GZU8	FAM192A	Protein FAM192A	1.225214573
Q8WXX5	DNAJC9	DnaJ homolog subfamily C member 9	1.224468646
Q14241	ELOA	Elongin-A	1.22408387
Q96RU3	FNBP1	Formin-binding protein 1	1.223685746
Q92665	MRPS31	28S ribosomal protein S31, mitochondrial	1.22356098
Q7Z7A3	CTU1	Cytoplasmic tRNA 2-thiolation protein 1	1.222682175
Q5U5X0	LYRM7	Complex III assembly factor LYRM7	1.222460414
Q86SX3	TEDC1	Tubulin epsilon and delta complex protein 1	1.222402928
Q9Y605	MRFAP1	MORF4 family-associated protein 1	1.222054027
P67809	YBX1	Nuclease-sensitive element-binding protein 1	1.221098797
Q15056	EIF4H	Eukaryotic translation initiation factor 4H	1.22035531
P16104	H2AFX	Histone H2AX	1.220301231
Q6P597	KLC3	Kinesin light chain 3	1.220071365
O75438	NDUFB1	NADH dehydrogenase [ubiquinone] 1 beta subcomplex subunit 1	1.218323423

O43869	OR2T1	Olfactory receptor 2T1	1.217257355
Q92890	UFD1	Ubiquitin recognition factor in ER-associated degradation protein 1	1.217034001
P49914	MTHFS	5-formyltetrahydrofolate cyclo-ligase	1.21680543
Q13310	PABPC4	Polyadenylate-binding protein 4	1.215944278
P62979	RPS27A	Ubiquitin-40S ribosomal protein S27a	1.215538359
P39019	RPS19	40S ribosomal protein S19	1.215411145
P11217	PYGM	Glycogen phosphorylase, muscle form	1.215091025
Q5T0J7	TEX35	Testis-expressed protein 35	1.214670339
P17844	DDX5	Probable ATP-dependent RNA helicase DDX5	1.214432238
P62854	RPS26	40S ribosomal protein S26	1.213852162
P04350	TUBB4A	Tubulin beta-4A chain	1.21345528
P52739	ZNF131	Zinc finger protein 131	1.213255521
P0DP23	CALM1	Calmodulin-1	1.212858704
O95858	TSPAN15	Tetraspanin-15	1.212515434
P49321	NASP	Nuclear autoantigenic sperm protein	1.212290647
Q92804	TAF15	TATA-binding protein-associated factor 2N	1.212153376
Q9UEW8	STK39	STE20/SPS1-related proline-alanine-rich protein kinase	1.211975842
P37108	SRP14	Signal recognition particle 14 kDa protein	1.211563615
P11387	TOP1	DNA topoisomerase 1	1.210311639
Q8NC51	SERBP1	Plasminogen activator inhibitor 1 RNA-binding protein	1.210131801
Q9NQ29	LUC7L	Putative RNA-binding protein Luc7-like 1	1.209813614
Q13185	CBX3	Chromobox protein homolog 3	1.209017436
Q9UHA3	RSL24D1	Probable ribosome biogenesis protein RLP24	1.208673628
P61586	RHOA	Transforming protein RhoA	1.208087113
P63173	RPL38	60S ribosomal protein L38	1.207837288
P31689	DNAJA1	DnaJ homolog subfamily A member 1	1.207619163
Q8NDD1	C1orf131	Uncharacterized protein C1orf131	1.207311341
Q8NEZ3	WDR19	WD repeat-containing protein 19	1.206519718
Q13228	SELENBP1	Methanethiol oxidase	1.206085953
Q15818	NPTX1	Neuronal pentraxin-1	1.205786198
Q96C90	PPP1R14B	Protein phosphatase 1 regulatory subunit 14B	1.204824062
Q8NEY1	NAV1	Neuron navigator 1	1.204636013
Q96F63	CCDC97	Coiled-coil domain-containing protein 97	1.20449852
O43252	PAPSS1	Bifunctional 3'-phosphoadenosine 5'-phosphosulfate synthase 1	1.204028572
Q3T8J9	GON4L	GON-4-like protein	1.203576735
Q9H5V9	CXorf56	UPF0428 protein CXorf56	1.203145848
O95817	BAG3	BAG family molecular chaperone regulator 3	1.203083931
Q16626	MEA1	Male-enhanced antigen 1	1.202481142
Q9Y3B7	MRPL11	39S ribosomal protein L11, mitochondrial	1.202303557
P39687	ANP32A	Acidic leucine-rich nuclear phosphoprotein 32 family member A	1.202219384
Q9Y4P1	ATG4B	Cysteine protease ATG4B	1.202163735
P02545	LMNA	Prelamin-A/C	1.201932112
O14979	HNRNPDL	Heterogeneous nuclear ribonucleoprotein D-like	1.201834809

P35269	GTF2F1	General transcription factor IIF subunit 1	1.201700967
Q9NRG1	PRTFDC1	Phosphoribosyltransferase domain-containing protein 1	1.201408167
P62829	RPL23	60S ribosomal protein L23	1.201268576
Q13885	TUBB2A	Tubulin beta-2A chain	1.200466376
Q66PJ3	ARL6IP4	ADP-ribosylation factor-like protein 6-interacting protein 4	1.200172608
Q3ZAQ7	VMA21	Vacuolar ATPase assembly integral membrane protein VMA21	0.832782621
Q9BUM1	G6PC3	Glucose-6-phosphatase 3	0.832725967
O94923	GLCE	D-glucuronyl C5-epimerase	0.832186111
Q7Z5Q5	POLN	DNA polymerase nu	0.831617641
P20742	PZP	Pregnancy zone protein	0.83152963
Q96RD7	PANX1	Pannexin-1	0.831370269
Q8TE02	ELP5	Elongator complex protein 5	0.831121022
Q7L3T8	PARS2	Probable proline--tRNA ligase, mitochondrial	0.8310823
P46977	STT3A	Dolichyl-diphosphooligosaccharide--protein glycosyltransferase subunit STT3A	0.830559413
P78540	ARG2	Arginase-2, mitochondrial	0.830279359
Q9H9S5	FKRP	Fukutin-related protein	0.830261536
P00846	MT-ATP6	ATP synthase subunit a	0.829722048
Q9H3Z4	DNAJC5	DnaJ homolog subfamily C member 5	0.829547542
Q96E22	NUS1	Dehydrodolichyl diphosphate synthase complex subunit NUS1	0.829483844
O43915	VEGFD	Vascular endothelial growth factor D	0.828244645
Q9BRT2	UQCC2	Ubiquinol-cytochrome-c reductase complex assembly factor 2	0.827465918
Q9H5Q4	TFB2M	Dimethyladenosine transferase 2, mitochondrial	0.827235437
Q8NFV4	ABHD11	Protein ABHD11	0.826893135
Q86W28	NLRP8	NACHT, LRR and PYD domains-containing protein 8	0.826277232
Q9P0S3	ORMDL1	ORM1-like protein 1	0.826062828
Q14118	DAG1	Dystroglycan	0.825977351
Q9NXN4	GDAP2	Ganglioside-induced differentiation-associated protein 2	0.825404298
Q5BJH2	TMEM128	Transmembrane protein 128	0.824934367
Q92609	TBC1D5	TBC1 domain family member 5	0.823697208
Q5BJF2	TMEM97	Sigma intracellular receptor 2	0.823311651
P43003	SLC1A3	Excitatory amino acid transporter 1	0.823250869
P56282	POLE2	DNA polymerase epsilon subunit 2	0.823130724
Q8WV93	AFG1L	AFG1-like ATPase	0.823080349
P09493	TPM1	Tropomyosin alpha-1 chain	0.823067091
Q15051	IQCB1	IQ calmodulin-binding motif-containing protein 1	0.82273043
Q9H553	ALG2	Alpha-1,3/1,6-mannosyltransferase ALG2	0.821977555
Q15904	ATP6AP1	V-type proton ATPase subunit S1	0.821957119
Q8WV99	ZFAND2B	AN1-type zinc finger protein 2B	0.821795463
O00767	SCD	Acyl-CoA desaturase	0.818973335
Q14728	MFSD10	Major facilitator superfamily domain-containing protein 10	0.818263868

O43657	TSPAN6	Tetraspanin-6	0.817291474
P42262	GRIA2	Glutamate receptor 2	0.817046231
Q9UIS9	MBD1	Methyl-CpG-binding domain protein 1	0.816872887
Q9UFH2	DNAH17	Dynein heavy chain 17, axonemal	0.815786939
Q96GJ1	TRMT2B	tRNA (uracil(54)-C(5))-methyltransferase homolog	0.814785738
Q07075	ENPEP	Glutamyl aminopeptidase	0.814424154
Q9H9H4	VPS37B	Vacuolar protein sorting-associated protein 37B	0.813843603
P61803	DAD1	Dolichyl-diphosphooligosaccharide--protein glycosyltransferase subunit DAD1	0.813294932
Q7Z3Z4	PIWIL4	Piwi-like protein 4	0.812560233
Q8NHP8	PLBD2	Putative phospholipase B-like 2	0.812152256
Q8N2K0	ABHD12	Monoacylglycerol lipase ABHD12	0.812047838
P07996	THBS1	Thrombospondin-1	0.811844003
O75449	KATNA1	Katanin p60 ATPase-containing subunit A1	0.811064652
Q12770	SCAP	Sterol regulatory element-binding protein cleavage-activating protein	0.811015248
Q9P2W1	PSMC3IP	Homologous-pairing protein 2 homolog	0.810824422
O00584	RNASET2	Ribonuclease T2	0.810520464
Q9NRM1	ENAM	Enamelin	0.810374692
P56134	ATP5J2	ATP synthase subunit f, mitochondrial	0.809812941
Q69YH5	CDCA2	Cell division cycle-associated protein 2	0.809240805
Q15118	PDK1	[Pyruvate dehydrogenase (acetyl-transferring)] kinase isozyme 1, mitochondrial	0.807523833
P18085	ARF4	ADP-ribosylation factor 4	0.807086646
Q5JSL3	DOCK11	Dedicator of cytokinesis protein 11	0.805761678
Q14108	SCARB2	Lysosome membrane protein 2	0.804760212
Q9H6K4	OPA3	Optic atrophy 3 protein	0.804190461
Q9Y221	NIP7	60S ribosome subunit biogenesis protein NIP7 homolog	0.803863387
Q9H2D1	SLC25A32	Mitochondrial folate transporter/carrier	0.803467367
Q86TJ2	TADA2B	Transcriptional adapter 2-beta	0.803350941
P12645	BMP3	Bone morphogenetic protein 3	0.802466945
Q8WTV0	SCARB1	Scavenger receptor class B member 1	0.801482955
Q9Y6K0	CEPT1	Choline/ethanolaminephosphotransferase 1	0.801353643
P12235	SLC25A4	ADP/ATP translocase 1	0.79831037
Q16563	SYPL1	Synaptophysin-like protein 1	0.798075113
P13645	KRT10	Keratin, type I cytoskeletal 10	0.797779412
Q9Y3E0	GOLT1B	Vesicle transport protein GOT1B	0.797708279
P02549	SPTA1	Spectrin alpha chain, erythrocytic 1	0.797692713
O43861	ATP9B	Probable phospholipid-transporting ATPase IIB	0.797331906
Q8IZ40	RCOR2	REST corepressor 2	0.797242036
Q99640	PKMYT1	Membrane-associated tyrosine- and threonine-specific cdc2-inhibitory kinase	0.797195019
Q8N3A8	PARP8	Poly [ADP-ribose] polymerase 8	0.797117318
Q9Y5B6	PAXBP1	PAX3- and PAX7-binding protein 1	0.795897418
Q8IV08	PLD3	Phospholipase D3	0.793494531
P32926	DSG3	Desmoglein-3	0.792615884

Q9Y3C1	NOP16	Nucleolar protein 16	0.78827528
Q9H3U5	MFSD1	Major facilitator superfamily domain-containing protein 1	0.787879985
P18440	NAT1	Arylamine N-acetyltransferase 1	0.787215966
Q0P6H9	TMEM62	Transmembrane protein 62	0.787004516
Q6IE37	OVOS1	Ovostatin homolog 1	0.785739729
P14854	COX6B1	Cytochrome c oxidase subunit 6B1	0.78573252
Q7LGC8	CHST3	Carbohydrate sulfotransferase 3	0.785139337
Q9UIU6	SIX4	Homeobox protein SIX4	0.785034589
Q8NF50	DOCK8	Dedicator of cytokinesis protein 8	0.783660065
P35527	KRT9	Keratin, type I cytoskeletal 9	0.777007683
Q9NVV0	TMEM38B	Trimeric intracellular cation channel type B	0.776968774
Q8WV60	PTCD2	Pentatricopeptide repeat-containing protein 2, mitochondrial	0.774537651
P55160	NCKAP1L	Nck-associated protein 1-like	0.769948494
A6NJI9	LRRC72	Leucine-rich repeat-containing protein 72	0.769321389
Q96E29	MTERF3	Transcription termination factor 3, mitochondrial	0.7684804
Q14703	MBTPS1	Membrane-bound transcription factor site-1 protease	0.764019643
Q8WV22	NSMCE1	Non-structural maintenance of chromosomes element 1 homolog	0.762571266
P02533	KRT14	Keratin, type I cytoskeletal 14	0.762261094
Q99683	MAP3K5	Mitogen-activated protein kinase kinase kinase 5	0.760636019
Q8N2E2	VWDE	von Willebrand factor D and EGF domain-containing protein	0.75919479
Q658P3	STEAP3	Metalloreductase STEAP3	0.754495043
Q9NR77	PXMP2	Peroxisomal membrane protein 2	0.75430007
Q9H061	TMEM126A	Transmembrane protein 126A	0.753290141
A2RU67	FAM234B	Protein FAM234B	0.751353893
Q9Y5L4	TIMM13	Mitochondrial import inner membrane translocase subunit Tim13	0.746474784
O75385	ULK1	Serine/threonine-protein kinase ULK1	0.742344796
Q9BY50	SEC11C	Signal peptidase complex catalytic subunit SEC11C	0.740168839
P02042	HBD	Hemoglobin subunit delta	0.738533281
Q14534	SQLE	Squalene monooxygenase	0.738456958
P30536	TSPO	Translocator protein	0.734624502
Q9P2K6	KLHL42	Kelch-like protein 42	0.733512268
P02768	ALB	Serum albumin	0.731421853
Q4W5G0	TIGD2	Tigger transposable element-derived protein 2	0.729096849
Q6UX72	B3GNT9	UDP-GlcNAc:betaGal beta-1,3-N-acetylglucosaminyltransferase 9	0.716845933
Q96BM9	ARL8A	ADP-ribosylation factor-like protein 8A	0.715510626
P57057	SLC37A1	Glucose-6-phosphate exchanger SLC37A1	0.713464264
Q9UJX2	CDC23	Cell division cycle protein 23 homolog	0.710770783
O15050	TRANK1	TPR and ankyrin repeat-containing protein 1	0.708247483
Q02413	DSG1	Desmoglein-1	0.707750707
P28330	ACADL	Long-chain specific acyl-CoA dehydrogenase, mitochondrial	0.707497167

P80365	HSD11B2	Corticosteroid 11-beta-dehydrogenase isozyme 2	0.700629987
Q9P003	CNIH4	Protein cornichon homolog 4	0.696978494
Q92564	DCUN1D4	DCN1-like protein 4	0.691796699
Q9NX00	TMEM160	Transmembrane protein 160	0.685147795
Q96EU6	RRP36	Ribosomal RNA processing protein 36 homolog	0.680711277
P78332	RBM6	RNA-binding protein 6	0.656667186
P04264	KRT1	Keratin, type II cytoskeletal 1	0.656660409
P21860	ERBB3	Receptor tyrosine-protein kinase erbB-3	0.643736939
P08779	KRT16	Keratin, type I cytoskeletal 16	0.633121401
Q5HY64	FAM47C	Putative protein FAM47C	0.625502861
P13647	KRT5	Keratin, type II cytoskeletal 5	0.611197075
P51786	ZNF157	Zinc finger protein 157	0.586087661
P48668	KRT6C	Keratin, type II cytoskeletal 6C	0.56390028
Q92858	ATOH1	Protein atonal homolog 1	0.561748688
Q9UL62	TRPC5	Short transient receptor potential channel 5	0.560397651
P78369	CLDN10	Claudin-10	0.553699125
Q9H8M5	CNNM2	Metal transporter CNNM2	0.537252179
O95674	CDS2	Phosphatidate cytidylyltransferase 2	0.490415498